2022 IEEE International Symposium on Electromagnetic Compatibility & Signal/Power Integrity (EMCSI) | 978-1-6654-0929-2/22/$31.00 ©2022 IEEE | DOI: 10.1109/EMCSI39492.2022.9889518

On the Vectorial Property of Stochastic Dyadic Green's Function in Complex Electronic Enclosures

Shen Lin, Yang Shao, Zhen Peng
Dept. Electrical and Computer Engineering
University of Illinois at Urbana-Champaign
Urbana, IL 61801 USA.
{shenlin2, yangshao, zvpeng}@illinois.edu

***Abstract*—This paper presents a physics-oriented, mathematically tractable statistical wave model for analyzing the naturally occurring chaotic dynamics of high-frequency reverberation within complex cavity environments. The key ingredient is a vector dyadic stochastic Green's function method derived from Wigner's random matrix theory and Berry's random wave hypothesis. The stochastic Green's function statistically replicates the multipath, ray-chaotic interactions between ports of entry and ports of interference without involving the complex details within the target's enclosure. The work achieves a physics-based modeling and simulation capability that predicts the probabilistic behavior of backdoor coupling to complex electronic enclosures.**

***Index Terms*—Chaos, electromagnetic coupling, Green function, intentional electromagnetic interference, statistical analysis**

I. Introduction

The study of electronics in strongly confined electromagnetic (EM) environments has been a longstanding topic in EM compatibility (EMC) and interference (EMI) community [1]–[5]. One well-known example is the mode-stirred reverberation chamber, which has been used as a standard laboratory facility for EMC testing [6]. Another important application is the intentional EMI (IEMI) to electronics hosted inside protective metallic enclosures (e.g. computer chassis, aircraft cabin). The external radio-frequency (RF) sources may penetrate into the target system through back-door channels such as seams, apertures, and cooling vents (so-called "ports of entry (POEs)"). The induced currents and voltages at the pins of internal electronics (so-called "ports of interference (POIs)") may disrupt the normal functionality of circuits components, resulting in either a short/long-term electronic upset or permanent damage, subject to increased levels of pulsed energy. As electronics are increasingly densely packed, working at higher frequencies, and operating at lower voltages, they are more sensitive and vulnerable to IEMI effects.

It is recognized that wave propagation inside electrically large enclosures may undergo multiple reflection/scattering from boundaries and internal structures, thus leading to randomized phase, polarization, and direction of wave fields. In the short wavelength limit, the wave scattering process may exhibit chaotic ray dynamics, albeit the underline wave equation is linear [7], [8]. From the eigenmode perspective, the complex boundary of the enclosure can lead to high modal density and high modal overlap. Under the high-frequency reverberation, the wave fields inside enclosures are very sensitive to the exact geometry of interior structures. Minor differences in the system configuration can result in significantly different EM field distributions inside the enclosure.

Given the complexity of such environments, it is crucial to develop stochastic models to account for the probabilistic nature of wave fields. Recently, a stochastic Green's function (SGF) approach [9] was introduced to model EM wave physics inside target enclosure with some approximately known information of cavity interior. At its heart, the SGF is based on a statistical description of the eigenmodes of an enclosed EM environment based on random matrix theory (RMT) [10]. Compared to related works, it rigorously separates the coherent and incoherent influences currents in one element have on fields of another element. Moreover, the statistics of the SGF are determined by generic, macroscopic properties of the cavity environment, including the operating frequency, cavity volume, loading, and wall losses.

In this paper, we present a stochastic dyadic Green's function approach as a means to relate the vector EM field to its source. The rationale behind this is that the variation and correlation of vectorial components are different at various locations, e.g. the center of the cavity, close to the wall, and close to the aperture. We have derived a mathematical framework accounting for all scenarios rigorously. The results provide solutions to three well-known problems of interest: (1) EM radiation in complex enclosures; (2) stochastic field-to-wire coupling; and (3) aperture coupling from an external plane wave.

II. Methodology

A. Derivation of Stochastic Dyadic Green's Function

Consider the 2^{nd} order vector wave equation in a cavity with reflecting boundary conditions, the vector dyadic Green's function for a source point at location $\mathbf{r}'$ satisfies,

$$\nabla \times \nabla \times \overline{\overline{\mathbf{G}}} - \omega^2 \mu\epsilon + j\omega\mu\sigma\overline{\overline{\mathbf{G}}}\left(\mathbf{r}, \mathbf{r}'\right) = -\overline{\overline{\mathbf{I}}}\delta\left(\mathbf{r} - \mathbf{r}'\right) \quad (1)$$

Note that σ is introduced to account for the energy losses occurring inside the cavity, i.e. lossy medium and imperfectly

The work is supported by U.S. NSF CAREER award, #1750839, and U.S. Office of Naval Research (ONR) Award #N00014-20-1-2835.

conducting walls. If we introduce the following notations: wavenumber $k = \omega\sqrt{\mu\epsilon}$, and cavity quality factor $Q = \omega\frac{\epsilon}{\sigma}$, the Green's function in the dyadic form can be constructed from the eigenfunction expansion [11], [12]:

$$\overline{\overline{\mathbf{G}}}_S(\mathbf{r},\mathbf{r}') = \sum_i \frac{\mathbf{\Psi}_i(\mathbf{r},k_i)\otimes\mathbf{\Psi}_i(\mathbf{r}',k_i)}{k^2-k_i^2-j\frac{k^2}{Q}} \tag{2}$$

where $\otimes$ indicates a tensor product. $\mathbf{\Psi}_i$ and k_i are the i^{th} vector eigenfunction and eigenvalue of the cavity. Namely, the radiation between source point $\mathbf{r}$ and receiving point $\mathbf{r}'$ is determined by a linear combination of orthogonal cavity eigenchannels. Whereas Equation 1 is in principle exact, it is impractical to compute these eigenfunctions and eigenvalues, due to the uncertainty and complexity of the environment.

Therefore, we prescribe substituting approximate, statistically defined eigenfunctions and eigenvalues. In particular, the eigenfunction statistics are derived from Berry's random wave model [13] and eigenvalues statistics generated by Wigner's random matrix theory [10]. Assuming both field and source points, $\mathbf{r}$, $\mathbf{r}'$ are away from the cavity boundary, the eigenfunction $\mathbf{\Psi}_i$ is approximated by a superposition of many plane waves with uniformly distributed orientation and polarization:

$$\mathbf{\Psi}_i(\mathbf{r},k_i) = \Psi_i^x(\mathbf{r})\,\hat{\mathbf{x}} + \Psi_i^y(\mathbf{r})\,\hat{\mathbf{y}} + \Psi_i^z(\mathbf{r})\,\hat{\mathbf{z}} \tag{3}$$

where the vector components are:

$$\Psi_i^x(\mathbf{r}) \simeq \lim_{N\to\infty}\sum_{n=1}^{N}[a_n(-\cos\psi_{pn}\sin\phi_n - \sin\psi_{pn}\cos\phi_n\cos\theta_n)\cos(k_i\hat{\mathbf{e}}_n\cdot\mathbf{r}+\beta_n)] \tag{4}$$

$$\Psi_i^y(\mathbf{r}) \simeq \lim_{N\to\infty}\sum_{n=1}^{N}[a_n(\cos\psi_{pn}\cos\phi_n - \sin\psi_{pn}\sin\phi_n\cos\theta_n)\cos(k_i\hat{\mathbf{e}}_n\cdot\mathbf{r}+\beta_n)] \tag{5}$$

$$\Psi_i^z(\mathbf{r}) \simeq \lim_{N\to\infty}\sum_{n=1}^{N}[a_n\sin\psi_{pn}\sin\theta_n\cos(k_i\hat{\mathbf{e}}_n\cdot\mathbf{r}+\beta_n)] \tag{6}$$

The polarization angle ψ_{pn}, direction $\hat{\mathbf{e}}_n$ and phase β_n are independent, uniform random variables. The amplitude a_n satisfies $\langle a_m a_n\rangle = \sqrt{\frac{2}{NV}}\delta_{mn}$.

The central limit theorem implies all Ψ_i^x, Ψ_i^y, and Ψ_i^z are mean-zero Gaussian random variables. To derive their variances, we replace the sum over the plane wave contributions by a continuous average over all directions for the propagation vector and polarizations. One can obtain the variances as: $\mathcal{V}_{xx} = \langle\Psi_i^x(\mathbf{r}),\Psi_i^x(\mathbf{r})\rangle = \frac{1}{3V}$, $\mathcal{V}_{yy} = \langle\Psi_i^y(\mathbf{r}),\Psi_i^y(\mathbf{r})\rangle = \frac{1}{3V}$, $\mathcal{V}_{zz} = \langle\Psi_i^z(\mathbf{r}),\Psi_i^z(\mathbf{r})\rangle = \frac{1}{3V}$, $\mathcal{V}_{xy} = \mathcal{V}_{xz} = \mathcal{V}_{yz} = 0$.

The next step is to derive the covariance between $\mathbf{\Psi}_i(\mathbf{r},k_i)$ and $\mathbf{\Psi}_i(\mathbf{r}',k_i)$. Without loss of generality, let $\mathbf{r}$ and $\mathbf{r}'$ located on the $\hat{\mathbf{z}}$ axis separating over a distance $R = |\mathbf{r}-\mathbf{r}'|$. The covariance function can be derived as:

$$\mathcal{C}_{xx}(R) = \langle\Psi_i^x(\mathbf{r}),\Psi_i^x(\mathbf{r}')\rangle = \frac{1}{3V}f_\perp(k_iR) \tag{7}$$

$$\mathcal{C}_{yy}(R) = \langle\Psi_i^y(\mathbf{r}),\Psi_i^y(\mathbf{r}')\rangle = \frac{1}{3V}f_\perp(k_iR) \tag{8}$$

$$\mathcal{C}_{zz}(R) = \langle\Psi_i^z(\mathbf{r}),\Psi_i^z(\mathbf{r}')\rangle = \frac{1}{3V}f_{//}(k_iR) \tag{9}$$

where $f_\perp(k_iR)$ and $f_{//}(k_iR)$ represent transversal and longitudinal correlation described by,

$$f_\perp(k_iR) = \frac{3}{2}\left[\frac{\sin k_iR}{k_iR} - \frac{\sin k_iR - k_iR\cos k_iR}{(k_iR)^3}\right] \tag{10}$$

$$f_{//}(k_iR) = 3\frac{\sin(k_iR) - k_iR\cos(k_iR)}{(k_iR)^3} \tag{11}$$

The results agree with the existing literature [14].

We can then reveal the statistical property of eigenfunctions with correlated Gaussian random variables using the discrete Karhunen-Loeve expansion [15]. The eigenfunctions are construed by correlated Gaussian random variables ω_i^x, ω_i^y, ω_i^z and $(\omega_i^x)'$, $(\omega_i^y)'$, $(\omega_i^z)'$, defined as:

$$\mathbf{\Psi}_i(\mathbf{r},k_i) \simeq \omega_i^x\hat{\mathbf{x}} + \omega_i^y\hat{\mathbf{y}} + \omega_i^z\hat{\mathbf{z}} \tag{12}$$

$$\mathbf{\Psi}_i(\mathbf{r}',k_i) \simeq (\omega_i^x)'\hat{\mathbf{x}} + (\omega_i^y)'\hat{\mathbf{y}} + (\omega_i^z)'\hat{\mathbf{z}} \tag{13}$$

where the covariance matrix of random variables is given by:

$$\begin{bmatrix} \mathcal{V}_{xx} & 0 & 0 & \mathcal{C}_{xx}(R) & 0 & 0 \\ 0 & \mathcal{V}_{yy} & 0 & 0 & \mathcal{C}_{yy}(R) & 0 \\ 0 & 0 & \mathcal{V}_{zz} & 0 & 0 & \mathcal{C}_{zz}(R) \\ \mathcal{C}_{xx}(R) & 0 & 0 & \mathcal{V}_{xx} & 0 & 0 \\ 0 & \mathcal{C}_{yy}(R) & 0 & 0 & \mathcal{V}_{yy} & 0 \\ 0 & 0 & \mathcal{C}_{zz}(R) & 0 & 0 & \mathcal{V}_{zz} \end{bmatrix}$$

Accordingly, the tensor product $\mathbf{\Psi}_i(\mathbf{r},k_i)\otimes\mathbf{\Psi}_i(\mathbf{r}',k_i)$ can be written in a dyadic expression:

$$\begin{aligned}\overline{\overline{\mathbf{D}}}(\mathbf{r},\mathbf{r}';k_i) = {}& \omega_i^x(\omega_i^x)'\hat{\mathbf{x}}\hat{\mathbf{x}} + \omega_i^x(\omega_i^y)'\hat{\mathbf{x}}\hat{\mathbf{y}} + \omega_i^x(\omega_i^z)'\hat{\mathbf{x}}\hat{\mathbf{z}} \\ & + \omega_i^y(\omega_i^x)'\hat{\mathbf{y}}\hat{\mathbf{x}} + \omega_i^y(\omega_i^y)'\hat{\mathbf{y}}\hat{\mathbf{y}} + \omega_i^y(\omega_i^z)'\hat{\mathbf{y}}\hat{\mathbf{z}} \\ & + \omega_i^z(\omega_i^x)'\hat{\mathbf{z}}\hat{\mathbf{x}} + \omega_i^z(\omega_i^y)'\hat{\mathbf{z}}\hat{\mathbf{y}} + \omega_i^z(\omega_i^z)'\hat{\mathbf{z}}\hat{\mathbf{z}}\end{aligned} \tag{14}$$

It is easy to show that the mean value of above dyadic is:

$$\left\langle\overline{\overline{\mathbf{D}}}(\mathbf{r},\mathbf{r}';k_i)\right\rangle = [\mathcal{C}_{xx}(R)\hat{\mathbf{x}}\hat{\mathbf{x}} + \mathcal{C}_{yy}(R)\hat{\mathbf{y}}\hat{\mathbf{y}} + \mathcal{C}_{zz}(R)\hat{\mathbf{z}}\hat{\mathbf{z}}] \tag{15}$$

Similar to the scalar SGF study, the stochastic dyadic Green's function can also be compared to the free-space dyadic Green's function. By substituting Eqs. (7)-(9) into (15), one can show that:

$$\left\langle\overline{\overline{\mathbf{D}}}(\mathbf{r},\mathbf{r}';k_i)\right\rangle = -\frac{2\pi}{kV}\mathrm{Im}\left[\overline{\overline{\mathbf{G}}}_0(\mathbf{r},\mathbf{r}';k_i)\right] \tag{16}$$

Therefore, the mean value of the stochastic dyadic SGF can be obtained as follows:

$$\begin{aligned}\left\langle\overline{\overline{\mathbf{G}}}_S(\mathbf{r},\mathbf{r}')\right\rangle &= \sum_i \frac{\left\langle\overline{\overline{\mathbf{D}}}(\mathbf{r},\mathbf{r}';k_i)\right\rangle}{k^2-k_i^2-j\frac{k^2}{Q}} \\ &= -\frac{1}{\pi}\sum_i \frac{\Delta(k_i^2)}{k^2-k_i^2-j\frac{k^2}{Q}}\mathrm{Im}\left[\overline{\overline{\mathbf{G}}}_0(\mathbf{r},\mathbf{r}';k_i)\right]\end{aligned} \tag{17}$$

where $\Delta(k_i^2) = 2\pi^2/(kV)$ is the average spacing between adjacent eigenvalues for 3D EM system. The sum over eigenmodes can then be written as a frequency-domain integral on average, and a statistically fluctuating contribution coming

from the denominator when eigenvalues $k_m \approx k$. By utilizing the Sokhotski-Plemelj theorem, we can rewrite Eq. 2 as:

$$\overline{\overline{\mathbf{G}}}_{\mathrm{S}}(\mathbf{r},\mathbf{r}') = \mathrm{Re}\left[\overline{\overline{\mathbf{G}}}_0(\mathbf{r},\mathbf{r}';k)\right] + \sum_m \frac{\overline{\overline{\mathbf{D}}}(\mathbf{r},\mathbf{r}';k_m)}{k^2 - k_m^2 - j\frac{k^2}{Q}} \quad (18)$$

Finally, the statistics of normalized eigenvalues to wavenumber $\left(k^2 - k_m^2\right)/\Delta\left(k_m^2\right)$ generated by the random matrix theory (RMT) [9]. The expression of stochastic dyadic Green's function (S-DGF) is given by:

$$\overline{\overline{\mathbf{G}}}_{\mathrm{S}}(\mathbf{r},\mathbf{r}') = \mathrm{Re}\left[\overline{\overline{\mathbf{G}}}_0(\mathbf{r},\mathbf{r}';k)\right] + \sum_m \frac{\overline{\overline{\mathbf{D}}}(\mathbf{r},\mathbf{r}';k_m)}{\tilde{\lambda}_m - j\alpha}\frac{kV}{2\pi^2} \quad (19)$$

where a macroscopic dimensionless loss-parameter, $\alpha = k^3V/\left(2\pi^2 Q\right)$ is introduced. The result of S-DGF will be utilized to analyze EM radiation problem in Sec. III. *A*.

B. Analysis of Wave Field close to Cavity Boundary

We note that in the derivation of S-DGF method, both source and receiving points are assumed to be away from cavity walls. Cavity eigenfunctions can thereby be locally approximated by an isotropic, random superposition of plane waves. It is clearly not the case in the evaluation of wave field close to cavity boundaries. Due to short-orbit couplings to close-by walls, the statistical properties of S-DGF are different from the uniform, isotropic case. In particular, when the field point is located at the highly conducting wall, the EM boundary condition needs to be satisfied exactly.

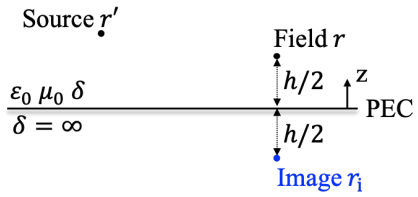

Fig. 1: Illustration of field point close to boundary

For illustration, we consider the case of source electric current located at $\mathbf{r}'$ radiating electric field inside a metallic cavity. The receiving point at $\mathbf{r}$ is close to a planar cavity wall on the xy plane, as shown in Fig. 1. To incorporate the reflected field from cavity wall, the random plane wave (RPW) approximation of eigenfunction in Eq. 3 is modified as:

$$\begin{aligned}\boldsymbol{\Psi}_i^{\mathrm{e}}(\mathbf{r}) \simeq\ & \tilde{\Psi}_i^x(\mathbf{r})\,\hat{\mathbf{x}} + \tilde{\Psi}_i^y(\mathbf{r})\,\hat{\mathbf{y}} + \tilde{\Psi}_i^z(\mathbf{r})\,\hat{\mathbf{z}} \\ & - \tilde{\Psi}_i^x(\mathbf{r}_{\mathrm{i}})\,\hat{\mathbf{x}} - \tilde{\Psi}_i^y(\mathbf{r}_{\mathrm{i}})\,\hat{\mathbf{y}} + \tilde{\Psi}_i^z(\mathbf{r}_{\mathrm{i}})\,\hat{\mathbf{z}}\end{aligned} \quad (20)$$

where $\mathbf{r}_{\mathrm{i}}\,(= x\hat{\mathbf{x}} + y\hat{\mathbf{y}} - z\hat{\mathbf{z}})$ denotes the image position of $\mathbf{r}\,(= x\hat{\mathbf{x}} + y\hat{\mathbf{y}} + z\hat{\mathbf{z}})$. Since $\tilde{\Psi}$ only consists of the plane waves propagating toward the boundary, $\left\langle \tilde{\Psi}_i^*, \tilde{\Psi}_i^* \right\rangle = \langle \Psi_i^*, \Psi_i^* \rangle/2$. The variances of vector components in $\boldsymbol{\Psi}_i^{\mathrm{e}}$ are derived as:

$$\mathcal{V}_{xx} = \left\langle \hat{\mathbf{x}}\cdot\boldsymbol{\Psi}_i^{\mathrm{e}}(\mathbf{r}), \hat{\mathbf{x}}\cdot\boldsymbol{\Psi}_i^{\mathrm{e}}(\mathbf{r}) \right\rangle = \frac{1}{3V}\left[1 - f_\perp(k_i h)\right] \quad (21)$$

$$\mathcal{V}_{yy} = \left\langle \hat{\mathbf{y}}\cdot\boldsymbol{\Psi}_i^{\mathrm{e}}(\mathbf{r}), \hat{\mathbf{y}}\cdot\boldsymbol{\Psi}_i^{\mathrm{e}}(\mathbf{r}) \right\rangle = \frac{1}{3V}\left[1 - f_\perp(k_i h)\right] \quad (22)$$

$$\mathcal{V}_{zz} = \left\langle \hat{\mathbf{z}}\cdot\boldsymbol{\Psi}_i^{\mathrm{e}}(\mathbf{r}), \hat{\mathbf{z}}\cdot\boldsymbol{\Psi}_i^{\mathrm{e}}(\mathbf{r}) \right\rangle = \frac{1}{3V}\left[1 + f_{//}(k_i h)\right] \quad (23)$$

Clearly, the variances in the transverse components and longitudinal behave differently. As the observation point $\mathbf{r}$ is far away from the boundary, all three cases reduce to the uniform case. At the wall boundary $z = 0$, we have: $\mathcal{V}_{xx} = \mathcal{V}_{yy} = 0$, $\mathcal{V}_{zz} = \frac{2}{3V}$. The tangential components are zero and the normal component is doubled, thereby the boundary condition of the eigenfunction is enforced.

To simplify the derivation of resulting vector SGF, we may rewrite the Eq. 20 as: $\boldsymbol{\Psi}_i^{\mathrm{e}}(\mathbf{r}) = \tilde{\boldsymbol{\Psi}}_i^{\mathrm{e}}(\mathbf{r}) - \tilde{\boldsymbol{\Psi}}_i^{\mathrm{e}}(\mathbf{r}_{\mathrm{i}}) + \hat{\mathbf{z}}\hat{\mathbf{z}}\cdot\tilde{\boldsymbol{\Psi}}_i^{\mathrm{e}}(\mathbf{r}_{\mathrm{i}})$. By following a similar procedure in Sec. II. *A* to derive the eigenfunction tensor product, $\boldsymbol{\Psi}_i^{\mathrm{e}}(\mathbf{r}) \otimes \boldsymbol{\Psi}_i(\mathbf{r}')$, we can obtain the vector dyadic SGF for the boundary electric field,

$$\overline{\overline{\mathbf{G}}}_S^{\mathrm{e,j}}(\mathbf{r},\mathbf{r}') = \overline{\overline{\mathbf{G}}}_S(\mathbf{r},\mathbf{r}') - \overline{\overline{\mathbf{G}}}_S(\mathbf{r}_{\mathrm{i}},\mathbf{r}') + 2\hat{\mathbf{z}}\hat{\mathbf{z}}\cdot\overline{\overline{\mathbf{G}}}_S(\mathbf{r}_{\mathrm{i}},\mathbf{r}') \quad (24)$$

The expression has an analogy with the well-know half-space electric dyadic Green's function of the first kind [16]. The result of Eq. 24 is utilized to analyze the stochastic field-to-wire coupling in Sec. III. *B*.

C. Analysis of Coupling to Cavities via Apertures

In many practical electronic systems, the enclosure maybe open to outside with multiple apertures at the cavity wall. Given an external RF radiation, the size and shape of the aperture determines the amount of EM power coupled into the cavity. Therefore, it is important to quantitatively study the site-specific aperture radiation and coupling [17]–[22].

Consider a cavity wall with an irregular aperture sitting in the xy plane, as illustrated in Fig. 2. The aperture is illuminated by an EM plane wave due to external RF sources. We start by introducing an artificial surface S_a over the aperture opening. The computational domain can then be decomposed into the interior confined cavity region and exterior host body region.

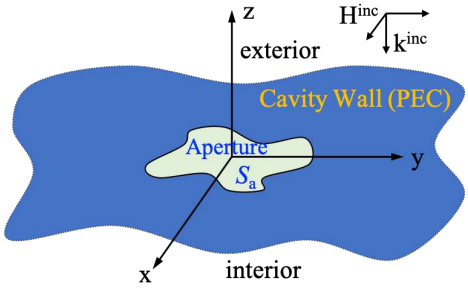

Fig. 2: Illustration for the aperture coupling problem

Based on the equivalence principle, the exterior subproblem can be formulated by a surface integral equation (SIE), whose unknowns involve the magnetic current $\mathbf{M}$ at the aperture [17]:

$$\mathbf{H}^+(\mathbf{r}) = 2\mathbf{H}^{\mathrm{inc}}(\mathbf{r}) + 2\frac{jk_0}{\eta}\iint_{S_a}\overline{\overline{\mathbf{G}}}_0(\mathbf{r},\mathbf{r}')\cdot\mathbf{M}(\mathbf{r}')\,dS' \quad (25)$$

To formulate the S-DGF of interior subproblem, we revise the RPW approximation of field eigenfunction $\boldsymbol{\Psi}_i^{\mathrm{h}}(\mathbf{r})$ as:

$$\begin{aligned}\boldsymbol{\Psi}_i^{\mathrm{h}}(\mathbf{r}) \simeq\ & \tilde{\Psi}_i^x(\mathbf{r})\,\hat{\mathbf{x}} + \tilde{\Psi}_i^y(\mathbf{r})\,\hat{\mathbf{y}} + \tilde{\Psi}_i^z(\mathbf{r})\,\hat{\mathbf{z}} \\ & + \tilde{\Psi}_i^x(\mathbf{r}_{\mathrm{i}})\,\hat{\mathbf{x}} + \tilde{\Psi}_i^y(\mathbf{r}_{\mathrm{i}})\,\hat{\mathbf{y}} - \tilde{\Psi}_i^z(\mathbf{r}_{\mathrm{i}})\,\hat{\mathbf{z}}\end{aligned} \quad (26)$$

A similar expression of RPW model is used for source eigenfunction $\mathbf{\Psi}_i^{\mathrm{m}}(\mathbf{r}')$. One can then derive the electric S-DGF of the second kind starting from the eigenfunction expansion:

$$\overline{\overline{\mathbf{G}}}_S^{\mathrm{h,m}}(\mathbf{r},\mathbf{r}') = \sum_i \frac{\mathbf{\Psi}_i^{\mathrm{h}}(\mathbf{r},k_i)\otimes\mathbf{\Psi}_i^{\mathrm{m}}(\mathbf{r}',k_i)}{k^2-k_i^2-j\frac{k^2}{Q}} \tag{27}$$

The details of the subsequent derivation are skipped for brevity. The resulting SIE for interior subproblem is given by:

$$\mathbf{H}^{-}(\mathbf{r}) = \frac{jk_0}{\eta}\iint_{S_a}\overline{\overline{\mathbf{G}}}_S^{\mathrm{h,m}}(\mathbf{r},\mathbf{r}')\cdot\mathbf{M}(\mathbf{r}')\,dS' \tag{28}$$

Through interface condition and Galerkin testing method [23], the surface IEs in Eqs. (25) and (28) can be casted into a matrix equation of the following form:

$$[\mathbf{Y}_0^{\mathrm{h,m}}+\mathbf{Y}_S^{\mathrm{h,m}}]\overline{\mathbf{M}} = \overline{\mathbf{H}}^{\mathrm{inc}} \tag{29}$$

where $\overline{\mathbf{H}}^{\mathrm{inc}}$ represents the excitation vector. $\mathbf{Y}_0^{\mathrm{h,m}}$ is the aperture admittance matrix for the exterior region in terms of free-space dyadic Green's function, whereas $\mathbf{Y}_S^{\mathrm{h,m}}$ is the aperture admittance matrix for the interior cavity region. The solution of aperture currents can then be used to analyze the statistics of transmitted power into the enclosure as well as the statistical shielding effectiveness. The variability is due to only approximately known information of interior cavity is used to construct the S-DGF model.

III. Validation and Verification

A. Electromagnetic Radiation in Wave-chaotic Enclosures

The first numerical study concerns an EM radiation problem with a pair of small electric dipoles as transmitter (Tx) and receiver (Rx). The goal is to evaluate the statistics of induced electric current at the Rx by changing its relative location and orientation. The results will be useful to assess fundamental EM radiation properties inside wave-chaotic enclosures.

The numerical experiment setup is illustrated in Fig. 3. Two small electric dipoles of length $l = 0.005\mathrm{m}$ are placed inside a 3D PEC enclosure and assumed to be far away from cavity wall. The Tx dipole is located at the origin with its wire directed along the x-axis. The current follows a triangular variation with the peak current at the center $I_0 = 400\mathrm{A}$. The operating frequency $f = 1.5\mathrm{GHz}$. The cavity environment is characterized by the macroscopic, dimensionless loss-parameter $\alpha = k^3V/\left(2\pi^2Q\right)$. Both dipoles are discretized by wire segments with the triangular basis function. The S-DGF is used to generate the IE matrices of the two antennas.

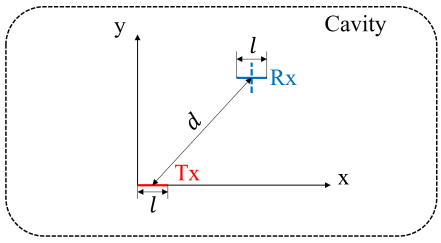

Fig. 3: Illustration of two small dipoles inside the cavity

1) The case of large separation: We consider first two electric dipole antennas are separated at a large distance, $d = 30\lambda$. As two dipoles are well-separated, the statistical behavior of S-DGF is dominated by the incoherent, diffusive coupling, which corresponds to wave propagation through many reflection/scattering paths inside the confined environment. The induced current at Rx antenna is expected to have uniform phase distribution and Rayleigh distributed amplitude [24], independent of the antenna orientation.

To confirm this assessment, we simulate two scenarios: one is the Rx dipole directed along the x-axis, and the other one is Rx dipole directed along the y-axis. The computed probability density function (PDF) of the induced current are plot in Fig. 4(a) and 4(b), respectively. The results confirm the theoretical assessment of Rayleigh distribution due to diffuse multipath scattering, irrespective of antenna orientation.

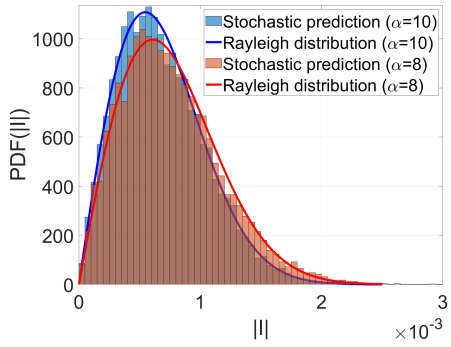

(a) x-directional Rx

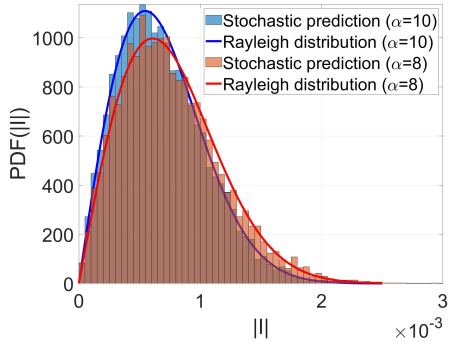

(b) y-directional Rx

Fig. 4: PDF of the amplitude of the current on the Rx dipole in the case of large separation.

2) The case of propagation correlation: To evaluate the proposed work in the case of propagation correlation, we adjust the distance between the two dipole antennas to 1λ. In this case, the orientation of the two dipoles should be considered. When the Rx dipole is placed along the x-axis, the coupling between the Tx and Rx dipoles includes both the coherent propagation of specular coupling and the incoherent, diffusive propagation. The result gives rise to a Rician distribution of induced current at the Rx dipole, as shown in Fig. 5(a). Whereas the Rx dipole is placed along y-axis, there is still no coherent propagation due to the prefect polarization mismatch.

Thus, the Raleigh distribution is observed in Fig. 5(b), similar to the case of large separation in Fig. 4.

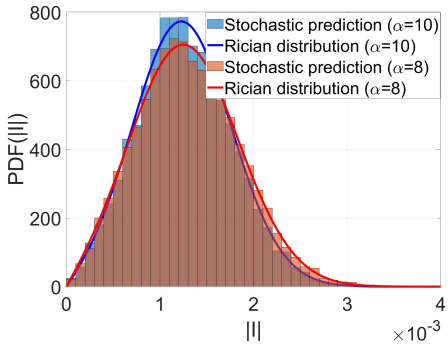

(a) x-directional Rx

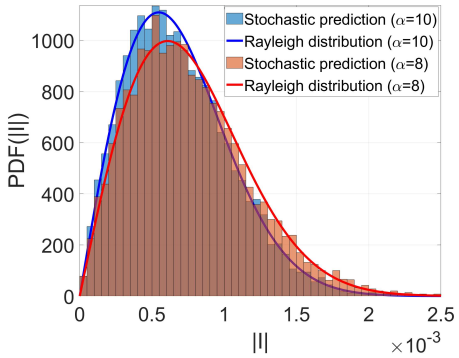

(b) y-directional Rx

Fig. 5: PDF of the amplitude of the current on the Rx dipole in the case of small separation.

B. Stochastic Field Coupling to a Conducting Wire

In the literature, the stochastic field-to-wire coupling has been studied theoretically and experimentally using reverberation chambers. For this validation, the mode-stirred chamber described in [25] is used. The dimensions of the chamber are $7.9\text{m} \times 6.5\text{m} \times 3.5\text{m}$. The U-shaped conducting wire has a length 1.1m and a 4mm^2 cross section. The distance between the parallel segment to the chamber wall is 32mm.

To replicate such a testing environment using the proposed work, a simulation setup shown in Fig. 6 is designed. The length L, height H, radius r are the same as the experimental setting. The wire is terminated with R_1=R_2=50Ω at both sides. A small dipole antenna is utilized to generate the stochastic field inside the cavity. By placing the dipole far away from the conducting wire, ($kD \geq \lambda$), we can utilize the S-DGF to calculate the power density of radiated diffusive field as: $\langle |\mathbf{E}|^2 \rangle = \frac{\omega^2 \mu^2 Q (I_0 l)^2}{24\pi k V}$. Next, based on the chamber constant (Fig. 3 in [25]) and quality factor (Fig. 4 in [26]), we can retrieve the dipole current $I_0 l$ that is needed to generate the same statistical cavity environment.

Both dipole and conducting wire are formulated by the electric field integral equation (EFIE) [27] with the S-DGF as kernel. A set of 5k Gaussian Orthogonal Ensemble (GOE) random matrices with dimension of 2000×2000 are used to generate S-DGF EFIE matrices. Thereby, 5k induced voltage samples at the wire terminals are computed with the proposed work. The mean of the squared magnitude $\langle |V|^2 \rangle$ is compared to measurement [25] in Fig. 7. A good agreement is observed.

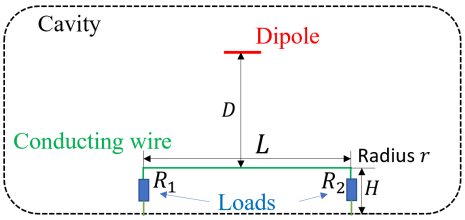

Fig. 6: Illustration of the radiated dipole and conducting wire

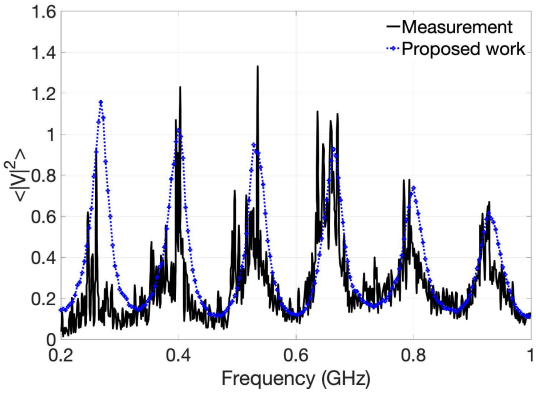

Fig. 7: Mean of the squared magnitude of coupled voltage

C. Aperture Coupling from External Plane Wave

To verify the aperture coupling from external plane wave, a complex, metallic computer chassis with various slots and opening on the cavity wall, as shown in the Fig. 8, was chosen as the test case. The aperture information is given in Table I. The computer chassis was illuminated by an external plane wave at 3GHz. The incident wave vector is k=(-1,0,0) and the electric field is along the +z direction.

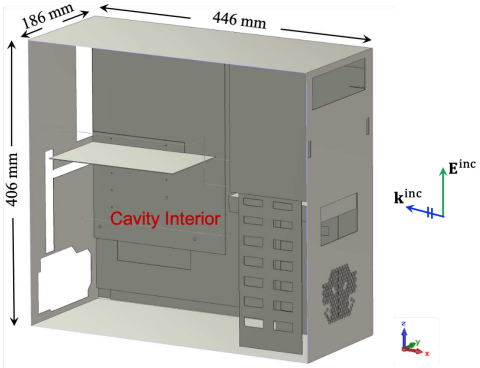

Fig. 8: The configuration of complex compute chassis

As there are internal losses in the computer chassis, the quality factor is determined by the leakage loss only. We first calculate the average leakage cross section using the EFIE

method formulated on the aperture surfaces. Together with the volume of the chassis, i.e. $V = 0.035\mathrm{m}^3$, the quality factor is obtained as $Q = 204.23$ and the loss-parameter $\alpha = 2.12$. The predicted cumulative distribution function (CDF) of internal E-fields are compared to the full-wave simulation results (by Monte Carlo sampling spatial data inside the computer chassis) in Fig. 9. Their corresponding mean values are also provided.

TABLE I: Aperture information for the computer chassis

	front-side		back-side	
	Length (m)	Width (m)	Length (m)	Width (m)
1	0.148	0.045	0.103	0.055
2	0.159	0.045	0.147	0.122
3	-	-	0.145	0.083

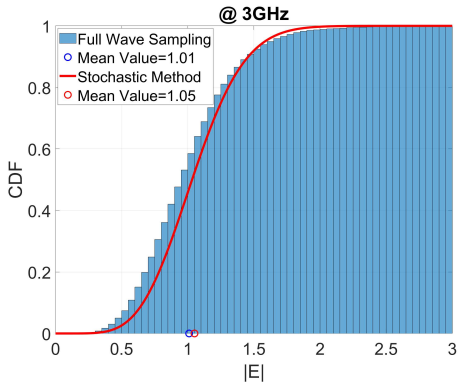

Fig. 9: The CDF of E-field amplitude for the computer chassis

IV. Conclusion

Due to increasingly complex electronic systems and continually evolving IEMI sources, it is expensive and impractical to perform experimental tests for all possible IEMI effects. Therefore, it identifies a timely and critical need for physics-oriented computational models, which characterize the fundamental wave physics of confined EM environments.

The key question answered in this work is, given the geometry/location of apertures and some approximately known information of interior cavity (volume, shape, quality factor, etc.), how can the statistics of the coupled internal EM fields and induced voltages at the interior electronics be predicted. We proposed a stochastic dyadic Green's function method, which integrated the deterministic (POEs and POIs) and statistical (cavity interior) attributes in a rigorous and comprehensive way.

References

[1] D. A. Hill, "Plane wave integral representation for fields in reverberation chambers," *IEEE Transactions on Electromagnetic Compatibility*, vol. 40, pp. 209–217, Aug 1998.

[2] V. Galdi, I. Pinto, and L. Felsen, "Wave propagation in ray-chaotic enclosures: paradigms, oddities and examples," *Antennas and Propagation Magazine, IEEE*, vol. 47, pp. 62–81, Feb 2005.

[3] A. Gifuni, "On the expression of the average power received by an antenna in a reverberation chamber," *IEEE Transactions on Electromagnetic Compatibility*, vol. 50, pp. 1021–1022, Nov 2008.

[4] S. Hemmady, T. Antonsen, E. Ott, and S. Anlage, "Statistical prediction and measurement of induced voltages on components within complicated enclosures: A wave-chaotic approach," *Electromagnetic Compatibility, IEEE Transactions on*, vol. 54, pp. 758–771, Aug 2012.

[5] J. C. West, R. Bakore, and C. F. Bunting, "Statistics of the current induced within a partially shielded enclosure in a reverberation chamber," *IEEE Transactions on Electromagnetic Compatibility*, vol. 59, no. 6, pp. 2014–2022, 2017.

[6] L. Arnaut, "Mode-stirred reverberation chambers: A paradigm for spatio-temporal complexity in dynamic electromagnetic environments," *Wave Motion*, vol. 51, no. 4, pp. 673 – 684, 2014. Innovations in Wave Modelling.

[7] G. Tanner and N. Sondergaard, "Wave chaos in acoustics and elasticity," *Journal of Physics A: Mathematical and Theoretical*, vol. 40, no. 50, p. R443, 2007.

[8] M. C. Gutzwiller, *Chaos in Classical and Quantum Mechanics (Interdisciplinary Applied Mathematics)*. New York: Springer, 1990.

[9] S. Lin, Z. Peng, and T. M. Antonsen, "A stochastic Green's function for solution of wave propagation in wave-chaotic environments," *IEEE Transactions on Antennas and Propagation*, vol. 68, no. 5, pp. 3919–3933, 2020.

[10] E. Wigner, "Random matrices in physics," *SIAM Review*, vol. 9, no. 1, pp. 1–23, 1967.

[11] J. Stein, H.-J. Stöckmann, and U. Stoffregen, "Microwave studies of billiard green functions and propagators," *Phys. Rev. Lett.*, vol. 75, pp. 53–56, Jul 1995.

[12] T. H. Lehman, "A statistical theory of electromagnetic fields in complex cavities," *EMP Interaction Note 494*, 1993.

[13] M. V. Berry, "Regular and irregular semiclassical wavefunctions," *Journal of Physics A: Mathematical and General*, vol. 10, no. 12, p. 2083, 1977.

[14] B. Eckhardt, U. Drr, U. Kuhl, and H.-J. Stckmann, "Correlations of electromagnetic fields in chaotic cavities," *Europhysics Letters (EPL)*, vol. 46, pp. 134–140, apr 1999.

[15] A. Papoulis and S. U. Pillai, *Probability, Random Variables, and Stochastic Processes*. McGraw-Hill Higher Education, 4 ed., 2002.

[16] C. T. Tai, *Dyadic Green Functions in Electromagnetic Theory (2nd edition)*. Piscataway, NJ: IEEE Press, 1994.

[17] R. F. Harrington and J. R. Mautz, "Electromagnetic coupling through apertures by the generalized admittance approach," *Computer Physics Communications*, vol. 68, no. 1, pp. 19–42, 1991.

[18] D. A. Hill, M. T. Ma, A. R. Ondrejka, B. F. Riddle, M. L. Crawford, , and R. T. Johnk, "Aperture excitation of electrically large, lossy cavities," *IEEE Transactions on Electromagnetic Compatibility*, vol. 36, pp. 169–178, Aug 1994.

[19] C. Bunting and S.-P. Yu, "Field penetration in a rectangular box using numerical techniques: an effort to obtain statistical shielding effectiveness," *IEEE Transactions on Electromagnetic Compatibility*, vol. 46, no. 2, pp. 160–168, 2004.

[20] R. Araneo and G. Lovat, "Fast mom analysis of the shielding effectiveness of rectangular enclosures with apertures, metal plates, and conducting objects," *IEEE Transactions on Electromagnetic Compatibility*, vol. 51, no. 2, pp. 274–283, 2009.

[21] A. Schroder, G. A. Rasek, H. Bruns, Z. Reznicek, J. Kucera, S. E. Loos, and C. Schuster, "Analysis of high intensity radiated field coupling into aircraft using the method of moments," *IEEE Transactions on Electromagnetic Compatibility*, vol. 56, pp. 113–122, 2014.

[22] G. Gradoni, T. M. Antonsen, S. M. Anlage, and E. Ott, "A statistical model for the excitation of cavities through apertures," *IEEE Transactions on Electromagnetic Compatibility*, vol. 57, pp. 1049–1061, Oct 2015.

[23] Z. Peng, Y. Shao, H. Gao, S. Wang, and S. Lin, "High-fidelity, high-performance computational algorithms for intrasystem electromagnetic interference analysis of ic and electronics," *IEEE Transactions on Components, Packaging and Manufacturing Technology*, vol. 7, pp. 653–668, May 2017.

[24] R. Holland and R. John, *Statistical Electromagnetics*. Philadelphia: Taylor and Francis, 1999.

[25] M. Magdowski, S. Siddiqui, and R. Vick, "Measurement of the stochastic electromagnetic field coupling into transmission lines in a reverberation chamber," in *2012 ESA Workshop on Aerospace EMC*, pp. 1–6, 2012.

[26] M. Magdowski, B. R. Banjade, and R. Vick, "Measurement of the coupling to shielded cables above a ground plane in a reverberation chamber," in *2016 International Symposium on Electromagnetic Compatibility - EMC EUROPE*, pp. 234–239, 2016.

[27] J. M. Jin, *Theory and Computation of Electromagnetic Fields, 2nd Edition*. Hoboken, New Jersey: John Wiley & Sons, Inc., 2015.